Journal of Computational and Applied Mathematics 313 (2017) 410–426

Contents lists available at ScienceDirect

Journal of Computational and Applied Mathematics

journal homepage: www.elsevier.com/locate/cam

# Immersed finite element method for eigenvalue problem

Seungwoo Lee [a], Do Y. Kwak [a], Imbo Sim [b,*]

[a] Department of Mathematical Science, Korea Advanced Institute of Science and Technology, 34141 Daejeon, Republic of Korea

[b] National Institute for Mathematical Sciences, 34047 Daejeon, Republic of Korea

ARTICLE INFO

*Article history:*
Received 9 June 2015
Received in revised form 12 July 2016

*Keywords:*
Eigenvalue
Finite elements
Immersed interface

ABSTRACT

We consider the approximation of elliptic eigenvalue problem with an interface. The main aim of this paper is to prove the stability and convergence of an immersed finite element method (IFEM) for eigenvalues using Crouzeix–Raviart $P_1$-nonconforming approximation. We show that spectral analysis for the classical eigenvalue problem can be easily applied to our model problem. We analyze the IFEM for elliptic eigenvalue problems with an interface and derive the optimal convergence of eigenvalues. Numerical experiments demonstrate our theoretical results.

© 2016 Elsevier B.V. All rights reserved.

## 1. Introduction

In this paper, we consider the approximation of elliptic eigenvalue problems with an interface. The interface problems are often encountered in fluid dynamics, electromagnetics, and materials science [1–4]. The main difficulty in solving such problems is caused mainly by the non-smoothness of solution across the interface. One choice to overcome it is to use finite element methods based on fitted meshes along the interface. Another choice is to use unfitted meshes independent of interface geometry for the computational domain. One of the advantages of using unfitted meshes is that we do not need to generate a mesh each time in the case of a moving interface which reduces computational costs. In this respect, several numerical methods have been proposed for example an *immersed boundary method* (IBM), *extended finite element method* (XFEM), *immersed interface method* (IIM), and *immersed finite element method* (IFEM). The IBM was introduced by Peskin to simulate cardiac mechanics and associated blood flow [5]. This method employs Eulerian and Lagrangian variables on Cartesian mesh and curvilinear mesh and they are linked by a smooth approximation of the Dirac delta function [6,7]. The XFEM is developed by extending the classical finite element method by enriching the finite element space with additional degrees of freedom [8,9]. LeVeque and Li [10] introduced the IIM based on the finite difference method where the jump conditions are properly incorporated in the scheme. However, the resulting linear system of equation from this method may not be symmetric and positive definite [11]. As an alternative, the IFEM has been developed for solving interface problems with unfitted meshes [11]. A feature of IFEM is that local basis functions are constructed to satisfy the jump conditions without additional degrees of freedom. The method has been applied to various types of partial differential equations involving interface such as two-phase incompressible flows [12] and a linear elasticity problem with a perfectly bonded interface [13,14]. The related works in this direction can be found in [15–20] and references therein.

The purpose of this paper is to prove the stability and convergence of an immersed finite element method for eigenvalues using Crouzeix–Raviart $P_1$-nonconforming approximation [17]. As a model problem, we consider the eigenvalue problem

* Corresponding author.
*E-mail addresses:* woo528@kaist.ac.kr (S. Lee), kdy@kaist.ac.kr (D.Y. Kwak), imbosim@nims.re.kr (I. Sim).

http://dx.doi.org/10.1016/j.cam.2016.09.035
0377-0427/© 2016 Elsevier B.V. All rights reserved.

with an interface, i.e.

$$\begin{aligned} -\nabla\cdot(\beta\nabla u) &= \lambda u \quad \text{in } \Omega^+\cup\Omega^-,\\ [u]_\Gamma &= 0, \qquad \left[\beta\frac{\partial u}{\partial n}\right]_\Gamma = 0,\\ u &= 0 \quad \text{on } \partial\Omega, \end{aligned} \tag{1}$$

where $\Omega$ is a convex polygonal domain in $\mathbb{R}^2$ which is separated into two subdomains $\Omega^+$ and $\Omega^-$ by a $C^2$-interface $\Gamma=\partial\Omega^-\subset\Omega$ with $\Omega^+=\Omega\setminus\Omega^-$. The symbol $[\,\cdot\,]_\Gamma$ denotes the jump across $\Gamma$. The coefficient $\beta$ is bounded below and above by two positive constants,

$$0<\beta_1\le\beta\le\beta_2<\infty.$$

The $P_1$-nonconforming FEM is widely used in solving elliptic equations and is shown to be useful in solving the mixed formulation of elliptic problems [21] and the Stokes equations [22]. Recently, Kwak et al. [17] introduced an immersed FEM based on the piecewise $P_1$-nonconforming polynomials and they proved optimal orders of convergence.

There have been various mathematical studies of finite element methods for eigenvalue problems. A unified approach to a posteriori and a priori error analysis for finite element approximations of self-adjoint elliptic eigenvalue problems is presented in [23]. The convergence of an adaptive method for elliptic eigenvalue problems is proved in [24]. For a nonconforming approximation, Dari et al. [25] provide a posteriori error analysis of the eigenvalue. The study of mixed eigenvalue problems can be found in [26–28]. To our best knowledge, spectral and convergence analysis of IFEM for eigenvalue problems with an interface has not been done so far. It is worth emphasizing that the spectral properties of eigenvalue problems with interface play key roles in the analysis and simulation for more complicated problems such as fluid–structure interactions, moving interfaces and the numerical stability for PDEs.

In this work, we analyze the IFEM for elliptic eigenvalue problems with interface and derive the optimal convergence of eigenvalues. Furthermore, we show that spectral analysis for the classical eigenvalue problem can be easily applied to our model problem. In particular, the spectral approximation of Galerkin methods can be proved by using fundamental properties of compact operators in Banach space. Such an investigation originates from a series of papers of Osborn and Babuška [29,30]. It has been extended in [31,32] to estimate Galerkin approximations for noncompact operators. Further application to discontinuous Galerkin approximations has been developed by Buffa et al. [33]. We formulate the eigenvalue problem with interface in terms of compact operators in order to understand the spectral behavior. The analysis presented in this paper is carried out along the lines of Refs. [31,32].

The paper is structured as follows. In the next section, we give a brief review on $P_1$-nonconforming IFEM [17]. In Section 3, we introduce a modified version of IFEM with an additional term and formulate the eigenvalue problem with the interface. Section 4 contains the analysis of the spectral approximation which is proved to be spurious-free and complete. The approximation is proved by means of basic results from the theory of compact operator in Banach space. In Section 5 we derive the convergence rate of eigenvalues based on $P_1$-nonconforming IFEM. In Section 6, we demonstrate numerical experiments for a model problem which corroborate the theoretical results in the preceding sections. In the final section, we provide a summary of our results.

## 2. Preliminaries

We consider an elliptic interface problem corresponding to the model problem (1):

$$\begin{aligned} -\nabla\cdot(\beta\nabla u) &= f \quad \text{in } \Omega^+\cup\Omega^-,\\ [u]_\Gamma &= 0, \qquad \left[\beta\frac{\partial u}{\partial n}\right]_\Gamma = 0,\\ u &= 0 \quad \text{on } \partial\Omega. \end{aligned} \tag{2}$$

The weak formulation of the problem (2) is to find $u\in H_0^1(\Omega)$ such that

$$\int_\Omega \beta\nabla u\cdot\nabla v dx=\int_\Omega fv dx, \quad \forall v\in H_0^1(\Omega) \tag{3}$$

with $f\in L^2(\Omega)$.

We begin by introducing a Sobolev space which is convenient for describing the regularity of the solution of the elliptic interface problem (2). For a bounded domain $D$, we let $H^m(D)=W_2^m(D)$ be the usual Sobolev space of order $m$ with semi-norm and norm denoted by $|\cdot|_{m,D}$ and $\|\cdot\|_{m,D}$, respectively. For real $m\ge 0$, the space $H^m(D)$ is defined by interpolation [34]. We define the space

$$\widetilde{H}^{1+\alpha}(D):=\{u\in H^1(D)\ :\ u\in H^{1+\alpha}(D\cap\Omega^s), s=+,-\}\quad \text{for } 0<\alpha\le 1$$

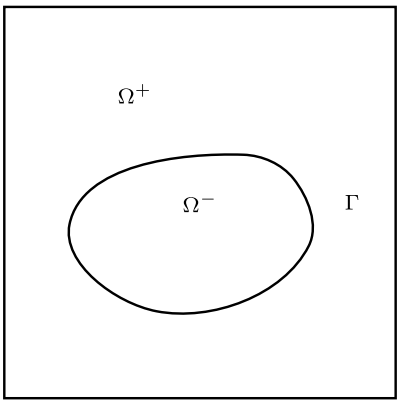


**Fig. 1.** A domain $\Omega$ with interface.

equipped with the norm

$$|u|^2_{\widetilde{H}^{1+\alpha}(D)} := |u|^2_{1+\alpha,D\cap\Omega^+} + |u|^2_{1+\alpha,D\cap\Omega^-},$$
$$\|u\|^2_{\widetilde{H}^{1+\alpha}(D)} := \|u\|^2_{1+\alpha,D\cap\Omega^+} + \|u\|^2_{1+\alpha,D\cap\Omega^-}.$$

Then we have following regularity theorem for the weak solution $u$ of the variational problem (3); see [35] and [36].

**Theorem 2.1.** *The variational problem (3) has a unique solution $u \in \widetilde{H}^{1+\alpha}(\Omega)$ which satisfies for some constant $C > 0$*

$$\|u\|_{\widetilde{H}^{1+\alpha}(\Omega)} \le C\|f\|_{0,\Omega},$$

*for some $\alpha \in (0, 1]$.*

We remark that the parameter $\alpha$ with respect to the regularity of the solution $u$ depends on the domain $\Omega$ and the interface $\Gamma$. As long as the domain is convex and the interface is smooth enough, the solution $u$ belongs to $\widetilde{H}^2(\Omega)$ [37]. Since the domain is convex polygonal and the interface is sufficiently smooth in our paper, we set $\alpha = 1$ (see Fig. 1).

Now describe an immersed finite element method (IFEM) based on Crouzeix–Raviart elements [17]. Let $\{\mathcal{K}_h\}$ be the usual quasi-uniform triangulations of the domain $\Omega$ by the triangles of maximum diameter $h$. Note that we do not require an element $K \in \mathcal{K}_h$ to be aligned with the interface $\Gamma$. We assume the following situations:

- (H1) the interface intersects the edges of an element at no more than two points
- (H2) the interface intersects each edge at most once, except possibly it passes through two vertices.

For a smooth interface, those assumptions are satisfied if mesh size $h$ is sufficiently small. We call an element $K \in \mathcal{K}_h$ an *interface element* if the interface $\Gamma$ passes through the interior of $K$, otherwise $K$ is a *non-interface element*. We denote by $\mathcal{K}_h^*$ the collection of all interface elements.

If we consider the problem in each subdomain, interface conditions are regarded as boundary conditions of elliptic problems in each subdomain. According to the works [35,38–41] which deal with the polygonal approximation of a smooth curved boundary, it suffices to consider the piecewise linear approximation of interface for our problem. We may replace $\Gamma \cap K$ by the line segment joining two intersection points on the edges of each $K \in \mathcal{K}_h^*$.

For each $K \in \mathcal{K}_h$ and non-negative integer $m$, let

$$\widetilde{H}^m(K) := \{u \in L^2(K) : u|_{K\cap\Omega^s} \in H^m(K \cap \Omega^s), s = +, -\},$$

equipped with norms

$$|u|^2_{m,K} := |u|^2_{m,K\cap\Omega^+} + |u|^2_{m,K\cap\Omega^-},$$
$$\|u\|^2_{m,K} := \|u\|^2_{m,K\cap\Omega^+} + \|u\|^2_{m,K\cap\Omega^-}.$$

To deal with the interface conditions in the model problem (1), we introduce the following spaces,

$$\widetilde{H}^2_\Gamma(K) := \left\{ u \in H^1(K) : u|_{K\cap\Omega^s} \in H^2(K \cap \Omega^s),\ s = +, - \text{ and } \left[\beta \frac{\partial u}{\partial n}\right]_\Gamma = 0 \text{ on } \Gamma \cap K \right\},$$
$$\widetilde{H}^2_\Gamma(\Omega) := \left\{ u \in H^1_0(\Omega) : u|_K \in \widetilde{H}^2_\Gamma(K),\ \forall K \in \mathcal{K}_h \right\}.$$

Clearly, $\widetilde{H}^2_\Gamma(K)$ and $\widetilde{H}^2_\Gamma(\Omega)$ are subspace of $\widetilde{H}^2(K)$ and $\widetilde{H}^2(\Omega)$, respectively.

As usual, we construct local basis functions on each element $K$ of the triangulation $\mathcal{K}_h$. We let

$$\overline{v}|_e = \frac{1}{|e|}\int_e v\, ds$$

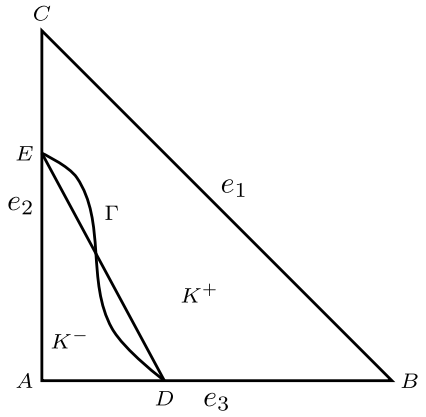


**Fig. 2.** A reference interface triangle.

denote the average of a function $v \in H^1(K)$ along an edge $e$. For a non-interface element $K \in \mathcal{K}_h$, we simply use the standard linear shape functions whose degrees of freedom are determined by average values on the edges. Let $N_h(K)$ denote the linear space spanned by the three basis functions $\phi_i$ satisfying $\overline{\phi_i}|_{e_j} = \delta_{ij}$ for $i, j = 1, 2, 3$. The $P_1$-nonconforming space $N_h(\Omega)$ is given by

$$N_h(\Omega) = \left\{ \phi : \phi|_K \in P_1(K) \text{ for } K \in \mathcal{K}_h \setminus \mathcal{K}_h^*; \text{ if } K_1, K_2 \in \mathcal{K}_h \text{ share an edge } e, \right. \\ \left. \text{then } \int_e \phi|_{\partial K_1} ds = \int_e \phi|_{\partial K_2} ds; \text{ and } \int_{\partial K \cap \partial\Omega} \phi \, ds = 0 \right\}.$$

Now we consider a reference interface element $K$ and assume that the interface $\Gamma$ intersects the edges of an element $K$ at $D$ and $E$ as in Fig. 2. Given linear basis functions $\phi_i$, $(i = 1, 2, 3)$ [22], we construct new basis functions $\hat{\phi}_i$ which hold the same degrees of freedom as $\phi_i$. Additionally, the functions $\hat{\phi}_i$ should be linear on $K^+$ and $K^-$, and satisfy the interface conditions in (1). The functions $\hat{\phi}_i$, $(i = 1, 2, 3)$ on the interface element $K$ can be described as follows:

$$\hat{\phi}_i = \begin{cases} c_1^- \phi_1 + c_2^- \phi_2 + c_3^- \phi_3 & \text{in } K^-, \\ c_1^+ \phi_1 + c_2^+ \phi_2 + c_3^+ \phi_3 & \text{in } K^+, \end{cases} \tag{4}$$

satisfying

$$\hat{\phi}_i^-(D) = \hat{\phi}_i^+(D), \qquad \hat{\phi}_i^-(E) = \hat{\phi}_i^+(E), \tag{5}$$

$$\frac{1}{|e_j|} \int_{e_j} \hat{\phi}_i \, ds = \delta_{ij}, \quad j = 1, 2, 3, \tag{6}$$

$$\overline{\beta^-} \frac{\partial \hat{\phi}_i^-}{\partial n}|_{\overline{DE}} = \overline{\beta^+} \frac{\partial \hat{\phi}_i^+}{\partial n}|_{\overline{DE}}, \tag{7}$$

where $\overline{\beta^-}$, $\overline{\beta^+}$ are the averages of the coefficient $\beta(x)$ over the segment $\overline{DE}$. The modified basis functions $\hat{\phi}_i$ are uniquely determined by (4)–(7) (see [17]).

We note that for a sharp interface, a violation of assumptions (H1) and (H2) may occur with even small $h$. Fig. 3 illustrates an example of a sharp interface. In this case, the way of constructing the modified IFEM basis functions (4)–(7) cannot be applied to elements $K_1$ and $K_2$ in Fig. 3.

We denote by $\widehat{N}_h(K)$ the local finite element space on the interface element $K$ whose basis functions $\hat{\phi}_i$, $i = 1, 2, 3$ are defined by above construction. We define the *immersed finite element space* $\widehat{N}_h(\Omega)$ as the collection of functions $\hat{\phi} \in L^2(\Omega)$ such that

- $\hat{\phi}|_K \in \widehat{N}_h(K)$ if $K \in \mathcal{K}_h^*$
- $\hat{\phi}|_K \in N_h(K)$ if $K \in \mathcal{K}_h \setminus \mathcal{K}_h^*$
- $\int_e \hat{\phi}|_{\partial K_1} ds = \int_e \hat{\phi}|_{\partial K_2} ds$ if $K_1, K_2 \in \mathcal{K}_h$ share an edge $e$
- $\int_{\partial K \cap \partial\Omega} \hat{\phi} \, ds = 0$.

Additionally let $H_h(\Omega) := H_0^1(\Omega) + \widehat{N}_h(\Omega)$ be endowed with the broken $H^1$-norm $\|v\|_{1,h}^2 := \sum_{K \in \mathcal{K}_h} \|v\|_{1,K}^2$.

We remark that the high-order IFEM for general curved interface is not reported yet to the best of authors' knowledge. Although the authors in [42] provide the construction of IFEM for nodal basis functions of higher order with extended jump conditions [42,43], they state that the construction is restricted to a linear interface and further investigation for approximation of curved interface is required.

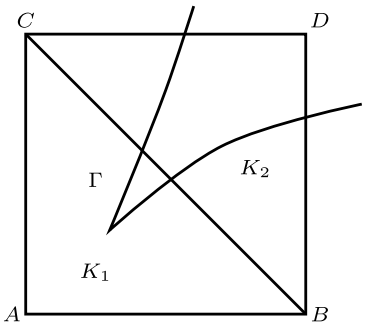


**Fig. 3.** Violation of assumptions (H1) and (H2).

## 3. Variational formulation

In this section, we consider a variational formulation for the model problem (1). Let $\Omega$ and $\Gamma$ be the same as in the previous section. In our analysis, we restrict the coefficient $\beta$ to be piecewise constant. Multiplying $v \in H_0^1(\Omega)$ and integrating by parts in $\Omega^{\pm}$, we obtain

$$\sum_{s=\pm}\int_{\Omega^s} -\nabla\cdot(\beta\nabla u)\cdot v\,dx = \sum_{s=\pm}\int_{\Omega^s}\beta\nabla u\cdot\nabla v\,dx - \int_{\Gamma}\left[\beta\frac{\partial u}{\partial n}\right]v\,dx$$
$$= \int_{\Omega}\beta\nabla u\cdot\nabla v\,dx.$$

Hence the weak formulation of the problem (1) is to find the eigenvalues $\lambda\in\mathbb{R}_+ := \{x\in\mathbb{R} : x>0\}$ and the eigenfunctions $u\in H_0^1(\Omega)$ such that

$$a(u,v) = \lambda(u,v), \quad \forall v\in H_0^1(\Omega), \tag{8}$$

where

$$a(u,v) = \int_{\Omega}\beta\nabla u\cdot\nabla v\,dx, \quad \forall u,v\in H_0^1(\Omega).$$

Since the bilinear form $a(\cdot,\cdot)$ is symmetric, continuous, and coercive on the space $H_0^1(\Omega)$, the eigenvalues $\lambda$ belong to $\mathbb{R}_+$. By a regularity property in Theorem 2.1, the eigenfunctions $u\in\widetilde{H}^2(\Omega)$. Using the solution operator $T : L^2(\Omega)\to H_0^1(\Omega)$, the eigenvalue problem (8) can be treated in terms of the variational form

$$a(Tf,v) = (f,v), \quad \forall v\in H_0^1(\Omega)$$

with $f\in L^2(\Omega)$. Note that if $(\lambda,u)\in\mathbb{R}_+\times H_0^1(\Omega)$ is an eigenpair of (8), then $(\lambda^{-1},\ u)$ is an eigenpair for the operator $T$.

For the application of IFEM to eigenvalue problems, we construct IFEM with a penalty term. We start by presenting a modified $P_1$-nonconforming IFEM for the elliptic problem (2). For some additional notations, let the collection of all the edges of $K\in\mathcal{K}_h$ be denoted by $\mathcal{E}_h$. We split $\mathcal{E}_h$ into two disjoint sets $\mathcal{E}_h = \mathcal{E}_h^o\cup\mathcal{E}_h^b$, where $\mathcal{E}_h^o$ is the set of edges lying in the interior of $\Omega$, and $\mathcal{E}_h^b$ is the set of edges on the boundary of $\Omega$.

The IFEM (modified by a penalty term) for (3) is to find $\hat{u}_h\in\widehat{N}_h(\Omega)$ such that

$$a_h^{\sigma}(\hat{u}_h,\hat{\phi}) = (f,\hat{\phi}), \quad \forall\hat{\phi}\in\widehat{N}_h(\Omega), \tag{9}$$

where

$$a_h^{\sigma}(u,v) := a_h(u,v) + j_{\sigma}(u,v),$$
$$a_h(u,v) := \sum_{K\in\mathcal{K}_h}\int_K\beta\nabla u\cdot\nabla v\,dx,$$
$$j_{\sigma}(u,v) := \sum_{e\in\mathcal{E}_h^o}\int_e\frac{\sigma}{h}[u]_e[v]_e\,ds, \text{ for some } \sigma>0.$$

We define the mesh dependent norm $\|\cdot\|_{1,J}$ on the space $H_h(\Omega)$ by

$$\|v\|_{1,J}^2 := \sum_{K\in\mathcal{K}_h}\|v\|_{0,K}^2 + \sum_{K\in\mathcal{K}_h}\|\nabla v\|_{0,K}^2 + \sum_{e\in\mathcal{E}_h^o}h^{-1}\|[v]\|_{0,e}^2.$$

By the trace inequality [44], this norm is equivalent to $\|\cdot\|_{1,h}$. For any penalty parameter $\sigma > 0$, the boundedness of the bilinear form $a_h^\sigma(\cdot,\cdot)$ can be shown easily by definition. The coerciveness of $a_h^\sigma(\cdot,\cdot)$ is obtained as follows. From [17], it holds that

$$a_h(v,v) \geq C \sum_{K\in\mathcal{K}_h} \|v\|_{0,K}^2, \quad \forall v \in \widehat{N}_h(\Omega),$$

where $C$ is a positive constant which is independent of mesh size $h$ and interface $\Gamma$ under the assumptions (H1) and (H2). We also have

$$a_h(v,v) \geq |\beta_{\min}| \sum_{K\in\mathcal{K}_h} \|\nabla v\|_{0,K}^2, \qquad j_\sigma(v,v) \geq \sigma \sum_{e\in\mathcal{E}_h^o} h^{-1}\|[v]\|_{0,e}^2.$$

Hence, the coerciveness and boundedness of the bilinear form $a_h^\sigma(\cdot,\cdot)$ are satisfied.

**Lemma 3.1.** *There exist positive constants $C_b$ and $C_c$ which are independent of interface under the assumptions* (H1) *and* (H2) *such that*

$$|a_h^\sigma(u,v)| \leq C_b\|u\|_{1,J}\|v\|_{1,J}, \quad \forall\, u, v \in H_h(\Omega),$$
$$a_h^\sigma(v,v) \geq C_c\|v\|_{1,J}^2, \qquad \forall\, v \in \widehat{N}_h(\Omega).$$

The following error estimate for (9) can be obtained by a slight modification of the proof in [17] by noting that $j_\sigma(u,v) = 0$ for any $u \in \widetilde{H}^2(\Omega)$ and $v \in \widehat{N}_h(\Omega)$.

**Theorem 3.2.** *Let $u \in \widetilde{H}^2(\Omega)$, $\hat{u}_h \in \widehat{N}_h(\Omega)$ be the solutions of (3) and (9), respectively. Assume that the solution $u$ satisfies $\beta\nabla u \in \left(H^1(\Omega)\right)^2$. Then there exists a constant $C > 0$ independent of the mesh size $h$ and the location of interface under the assumptions* (H1) *and* (H2) *such that*

$$\|u - \hat{u}_h\|_{0,\Omega} + h\|u - \hat{u}_h\|_{1,J} \leq Ch^2\|f\|_{0,\Omega}.$$

The IFEM for the eigenvalue problem (1) is to find the pairs $(\lambda_h, \hat{u}_h) \in \mathbb{R}_+ \times \widehat{N}_h(\Omega)$ such that

$$a_h^\sigma(\hat{u}_h, \hat{\phi}) = \lambda_h(\hat{u}_h, \hat{\phi}), \quad \forall \hat{\phi} \in \widehat{N}_h(\Omega).$$

Let us define the discrete solution operator $T_h : L^2(\Omega) \to \widehat{N}_h(\Omega)$ by

$$a_h^\sigma(T_hf, \hat{\phi}) = (f, \hat{\phi}), \quad \forall \hat{\phi} \in \widehat{N}_h(\Omega)$$

with $f \in L^2(\Omega)$. In view of the definition of the discrete solution operator $T_h$, the eigenvalues $\mu_h$ of the operator $T_h$ are given by $\mu_h = 1/\lambda_h$.

## 4. Spectral approximation

Now we are concerned with the spectral approximation that can be proved by using some properties of compact operators in Banach space. We follow the approaches given in [31,32].

Clearly, the operator $T$ is self-adjoint and bounded. Similarly, the operator $T_h$ is self-adjoint on $\widehat{N}_h(\Omega)$ such that

$$a_h^\sigma(T_hf, \phi) = a_h^\sigma(f, T_h\phi), \quad \forall f, \phi \in \widehat{N}_h(\Omega).$$

Next, the boundedness of the operator $T_h$ can be shown by using the coerciveness of the bilinear form $a_h^\sigma(\cdot,\cdot)$. For any $f \in L^2(\Omega)$, it holds that

$$\begin{aligned}\|T_hf\|_{1,J}^2 &\leq Ca_h^\sigma(T_hf, T_hf)\\ &= C(f, T_hf)\\ &\leq C\|f\|_{0,\Omega}\|T_hf\|_{0,\Omega}\\ &\leq C\|f\|_{0,\Omega}\|T_hf\|_{1,J}.\end{aligned}$$

Therefore, $\|T_hf\|_{1,J} \leq C\|f\|_{0,\Omega}$.

The operator $T$ is compact in $H_0^1(\Omega)$ due to the boundedness of $T$ and Rellich–Kondrachov theorem i.e. the compact embedding $H_0^1(\Omega) \subset L^2(\Omega)$ [34]. Clearly, the operator $T_h$ is compact in $H_h(\Omega)$ by the definition of $T_h$.

In order to obtain uniform convergence of $T_h$ to $T$ from Theorem 3.2, we assume $\beta\nabla(Tf) \in \left(H^1(\Omega)\right)^2$ for $f \in L^2(\Omega)$.

Let $\sigma(T)$ and $\rho(T)$ be the spectrum and resolvent set of $T$, respectively. The spectrum $\sigma(T)$ is a countable set with no accumulation points different from zero and consists of positive real eigenvalues with finite multiplicity [45]. The algebraic multiplicity of each eigenvalue $\mu \in \sigma(T)$ is equal to the geometric multiplicity due to the self-adjointness and compactness of the operator $T$ [45]. For any $z \in \rho(T)$, the resolvent operator $R_z(T)$ is defined by $R_z(T) = (z-T)^{-1}$ from $L^2(\Omega)$ to $L^2(\Omega)$ or from $H_0^1(\Omega)$ to $H_0^1(\Omega)$. Following Refs. [31,32], we prove the non-pollution of the spectrum. To do so, we need the following results.

**Lemma 4.1.** *For $z \in \rho(T)$, $z \neq 0$, there is a constant $C > 0$ depending on only $\Omega$ and $|z|$ such that*

$$\|(z - T)f\|_{1,J} \geq C\|f\|_{1,J}, \quad \forall f \in H_h(\Omega).$$

**Proof.** Let $g = (z - T)f$. We need to show $\|f\|_{1,J} \leq C\|g\|_{1,J}$. From the definition of $T$ and $g$, we have the equalities,

$$a(Tf, v) = a(zf - g, v) = (f, v), \quad \forall v \in H_0^1(\Omega). \tag{10}$$

Reformulating the second equality in (10), we obtain

$$a(zf - g, v) - \frac{1}{z}(zf - g, v) = \frac{1}{z}(g, v), \quad \forall v \in H_0^1(\Omega). \tag{11}$$

Since $z \in \rho(T)$, the inverse $z^{-1}$ is not an eigenvalue of $a(\cdot, \cdot)$. Hence $zf - g$ is the solution of the weak formulation (11). By using Theorem 2.1, we have

$$\|zf - g\|_{1,J} \leq C\frac{1}{|z|}\|g\|_{0,\Omega} \leq C\frac{1}{|z|}\|g\|_{1,J}. \tag{12}$$

From the triangle inequality and (12), it follows immediately that

$$\begin{aligned}\|f\|_{1,J} &\leq \frac{1}{|z|}(\|zf - g\|_{1,J} + \|g\|_{1,J}) \\ &\leq \frac{1}{|z|}\left(C\frac{1}{|z|}\|g\|_{1,J} + \|g\|_{1,J}\right) \\ &\leq C(|z|)\|g\|_{1,J}\ ,\end{aligned}$$

where $C(|z|)$ is a constant depending on $|z|$. □

**Theorem 4.2.** *For $z \in \rho(T)$, $z \neq 0$, there is a constant $C > 0$ depending only on $\Omega$ and $|z|$ such that for $h$ small enough*

$$\|(z - T_h)f\|_{1,J} \geq C\|f\|_{1,J}, \quad \forall f \in H_h(\Omega).$$

*In other words, the resolvent operator $R_z(T_h) = (z - T_h)^{-1}$ is bounded.*

**Proof.** By Theorem 3.2 and Lemma 4.1, we get

$$\begin{aligned}\|(z - T_h)f\|_{1,J} &\geq \|(z - T)f\|_{1,J} - \|(T - T_h)f\|_{1,J} \\ &\geq (C_1(|z|) - C_2h)\|f\|_{1,J} \\ &\geq C(|z|)\|f\|_{1,J},\end{aligned}$$

for $h$ small enough. □

Before we state the following Corollary, we denote an operator norm $\|L\|_{\mathscr{L}(X,Y)}$ for a bounded linear operator $L : X \to Y$ by

$$\|L\|_{\mathscr{L}(X,Y)} = \sup_{x \in X} \frac{\|Lx\|_Y}{\|x\|_X}. \tag{13}$$

**Corollary 4.3.** *Let $F \subset \rho(T)$ be closed, then*

$$\|R_z(T_h)\|_{\mathscr{L}(H_h(\Omega),H_h(\Omega))} \leq C, \quad \forall z \in F,$$

*for some constant $C$.*

The following result is a direct consequence of Corollary 4.3. We note that the proof is analogous to Theorem 1 in [31].

**Theorem 4.4** (*Non-Pollution of the Spectrum*)**.** *Let $A \subset \mathbb{R}_+$ be an open set containing $\sigma(T)$. Then for sufficiently small $h$, $\sigma(T_h) \subset A$.*

This implies that there are no discrete spurious eigenvalues of the solution operator $T_h$.

Now we turn to show the non-pollution and completeness of the eigenspace [31,32]. Let $\mu$ be an eigenvalue of $T$ with algebraic multiplicity $n$. We define the spectral projection $E(\mu)$ from $L^2(\Omega)$ into $H_0^1(\Omega)$ by

$$E(\mu) = \frac{1}{2\pi i}\int_\Lambda R_z(T)\, dz,$$

where $\Lambda$ is a Jordan curve in $\mathbb{C}$ containing $\mu$, which lies in $\rho(T)$ and does not enclose any other points of $\sigma(T)$ [45]. By Corollary 4.3, the discrete resolvent operator $R_z(T_h)$ is bounded. Therefore, we can define the discrete spectral projection $E_h(\mu)$ from $L^2(\Omega)$ into $H_h(\Omega)$ by

$$E_h(\mu) = \frac{1}{2\pi i}\int_{\Lambda} R_z(T_h)\, dz.$$

The projections $E(\mu)$ and $E_h(\mu)$ are simply denoted by $E$ and $E_h$, respectively. The following theorem provides the uniform convergence of spectral projections.

**Theorem 4.5.** *It holds that*

$$\lim_{h\to 0} \|E - E_h\|_{\mathcal{L}(L^2(\Omega),H_h(\Omega))} = 0.$$

**Proof.** By using the resolvent identity

$$R_z(T) - R_z(T_h) = R_z(T_h)(T - T_h)R_z(T),$$

we obtain for $f \in L^2(\Omega)$,

$$\begin{aligned}\|(E - E_h)f\|_{1,J} &\le C\|(R_z(T) - R_z(T_h))f\|_{1,J}\\ &= C\|R_z(T_h)(T - T_h)R_z(T)f\|_{1,J}\\ &\le C\|R_z(T_h)\|_{\mathcal{L}(H_h(\Omega),H_h(\Omega))}\|T - T_h\|_{\mathcal{L}(L^2(\Omega),H_h(\Omega))}\\ &\quad\cdot \|R_z(T)\|_{\mathcal{L}(L^2(\Omega),L^2(\Omega))}\|f\|_{L^2(\Omega)}.\end{aligned}$$

For $h$ small enough, $\|R_z(T_h)\|_{\mathcal{L}(H_h(\Omega),H_h(\Omega))}$ and $\|R_z(T)\|_{\mathcal{L}(L^2(\Omega),L^2(\Omega))}$ are bounded by Theorem 4.2 and Fredholm alternative [46], respectively. The operator norm $\|T-T_h\|_{\mathcal{L}(L^2(\Omega),H_h(\Omega))}$ goes to zero as $h \to 0$. The proof is now complete. □

We are now in a position to show the boundedness of the distance between eigenspaces. Such a distance for any closed subspaces of $H_h(\Omega)$ may be evaluated by means of distance functions

$$\operatorname{dist}_h(x, Y) = \inf_{y\in Y}\|x - y\|_{1,J}, \qquad \operatorname{dist}_h(Y, Z) = \sup_{y\in Y,\,\|y\|_{1,J}=1} \operatorname{dist}_h(y, Z),$$

$$\operatorname{dist}(Y, Z) = \max(\operatorname{dist}_h(Y, Z), \operatorname{dist}_h(Z, Y)).$$

The following results are analogous to Theorem 4.5, whose proofs can be obtained as in [31].

**Theorem 4.6.** • *(Non-pollution of the eigenspace)*

$$\lim_{h\to 0} \operatorname{dist}_h(E_h(H_h(\Omega)), E(H_0^1(\Omega))) = 0.$$

• *(Completeness of the eigenspace)*

$$\lim_{h\to 0} \operatorname{dist}_h(E(H_0^1(\Omega)), E_h(H_h(\Omega))) = 0.$$

It remains to show that the distance between the spectrums of $T$ and $T_h$ vanishes as $h$ goes to zero.

**Theorem 4.7** (*Completeness of the Spectrum*)**.** *For all $z \in \sigma(T)$,*

$$\lim_{h\to 0} \operatorname{dist}_h(z, \sigma(T_h)) = 0.$$

**Proof.** The proof follows from Theorem 6 in [31]. □

## 5. Convergence analysis

In this section, we present the convergence analysis of eigenvalues. By using the spectral properties of compact operators in the previous section, we show the convergence rate of eigenvalues.

**Theorem 5.1.** *Let $\mu$ be an eigenvalue of $T$ with multiplicity $n$. Assume that the corresponding eigenfunction $u$ satisfies $\beta\nabla u \in \left(H^1(\Omega)\right)^2$. Then for $h$ small enough there exist $n$ eigenvalues $\{\mu_{1,h}, \ldots, \mu_{n,h}\}$ of $T_h$ which converge to $\mu$ in such a way that*

$$\sup_{1\le i\le n} |\mu - \mu_{i,h}| \le Ch^2,$$

*where a positive constant $C$ is independent of $\mu$, the mesh size $h$, and the location of interface under the assumptions* (H1) *and* (H2) *.*

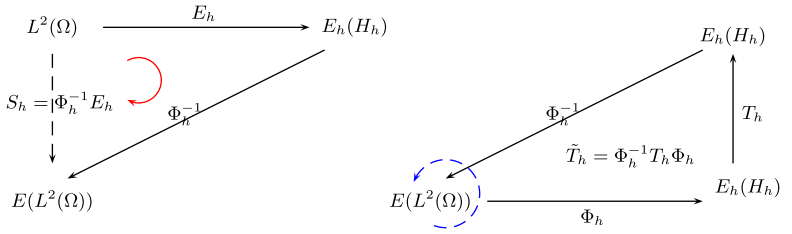


**Fig. 4.** The operators $S_h$ and $\tilde{T}_h$.

**Proof.** The existence of $\mu_{i,h}$ is a direct consequence of the previous section. Now we estimate the convergence rate of $\mu_{i,h}$. Let $\Phi_h$ be the restriction of $E_h$ to $E(L^2(\Omega))$:

$$\Phi_h = E_h|_{E(L^2(\Omega))} : E(L^2(\Omega)) \to E_h(H_h(\Omega)).$$

Following the arguments in [29,30], we can show that the inverse $\Phi_h^{-1} : E_h(H_h(\Omega)) \to E(L^2(\Omega))$ is bounded for $h$ small enough. To show $\Phi_h^{-1}$ is defined, let $\Phi_h f = 0$ with $f \in E(L^2(\Omega))$. Then by Theorem 4.5, we have

$$\|f\|_{0,\Omega} = \|f - \Phi_h f\|_{0,\Omega} = \|Ef - E_h f\|_{0,\Omega} \le \|E - E_h\|_{\mathscr{L}(L^2(\Omega),H_h(\Omega))} \|f\|_{0,\Omega}.$$

Thus $\Phi_h$ is one-to-one. By Theorem 4.6, $\Phi_h$ is onto such that the inverse $\Phi_h^{-1}$ is defined. Now we show that $\Phi_h^{-1}$ is bounded. For $f \in E(L^2(\Omega))$ and $h$ small enough,

$$\begin{aligned}
\|\Phi_h f\|_{0,\Omega} &\ge \|f\|_{0,\Omega} - \|f - \Phi_h f\|_{0,\Omega} \\
&= \|f\|_{0,\Omega} - \|Ef - E_h f\|_{0,\Omega} \\
&\ge (1 - \|E - E_h\|_{\mathscr{L}(L^2(\Omega),H_h(\Omega))}) \|f\|_{0,\Omega} \\
&\ge \frac{1}{2} \|f\|_{0,\Omega}.
\end{aligned}$$

Hence the inverse $\Phi_h^{-1}$ is bounded.

Let $\widetilde{T}$ be the restriction of $T$ to $E(L^2(\Omega))$ and define $\widetilde{T}_h := \Phi_h^{-1} T_h \Phi_h$. Setting $S_h = \Phi_h^{-1} E_h : L^2(\Omega) \to E(L^2(\Omega))$ (see Fig. 4), we see that $S_h$ is bounded and $S_h f = f$ for any $f \in E(L^2(\Omega))$. By definitions of $\widetilde{T}$, $\widetilde{T}_h$, $S_h$, $\Phi_h$, and the properties $T_h E_h = E_h T_h$ and $Tf \in E(L^2(\Omega))$, we have for any $f \in E(L^2(\Omega))$,

$$\begin{aligned}
(\widetilde{T} - \widetilde{T}_h) f &= Tf - \Phi_h^{-1} T_h \Phi_h f \\
&= S_h Tf - \Phi_h^{-1} T_h E_h f \\
&= S_h Tf - \Phi_h^{-1} E_h T_h f \\
&= S_h (T - T_h) f.
\end{aligned}$$

By definition of operator norm (13) and Theorem 3.2, we have

$$\begin{aligned}
\sup_{1 \le i \le n} |\mu - \mu_{i,h}| &\le C \|\widetilde{T} - \widetilde{T}_h\|_{\mathscr{L}(E(L^2(\Omega)),E(L^2(\Omega)))} \\
&= C \sup_{f \in E(L^2(\Omega))} \frac{\|(\widetilde{T} - \widetilde{T}_h) f\|_{0,\Omega}}{\|f\|_{0,\Omega}} \\
&= C \sup_{f \in E(L^2(\Omega))} \frac{\|S_h (T - T_h) f\|_{0,\Omega}}{\|f\|_{0,\Omega}} \\
&\le C \sup_{f \in E(L^2(\Omega))} \frac{\|(T - T_h) f\|_{0,\Omega}}{\|f\|_{0,\Omega}} \\
&\le C h^2 .
\end{aligned}$$

**Remark 1.** Theorem 5.1 can be expressed in terms of the eigenvalues $\lambda = \mu^{-1}$ and $\lambda_{i,h} = \mu_{i,h}^{-1}$ as

$$\frac{|\lambda - \lambda_{i,h}|}{|\lambda_{i,h}|} \le C_1 h^2.$$

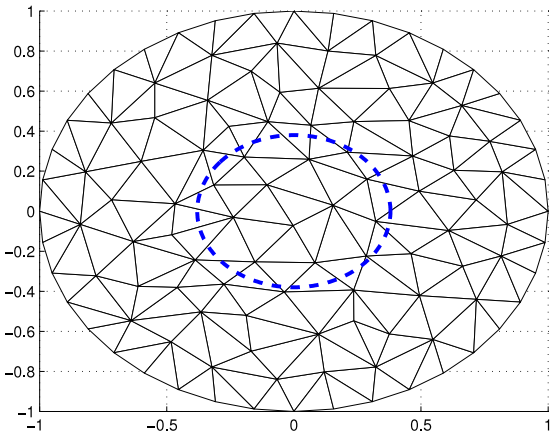


**Fig. 5.** Example of mesh generation. The inner broken line represents the interface $\Gamma$.

For $h$ small enough, we derive the estimate for the relative error

$$\frac{|\lambda - \lambda_{i,h}|}{|\lambda|} \leq \frac{C_1 h^2}{1 - C_1|\lambda| h^2} \leq Ch^2.$$

## 6. Numerical results

We demonstrate numerical experiments for our model problem (1). In the first example, we test an elliptic eigenvalue problem with a circular interface for which we know the exact eigensolutions. Next we perform experiments for the cases with star-shaped interface and straight-line interface. We observe the optimal orders of convergence of numerical eigenvalues. In our computations we use the package ARPACK [47] which is designed for solving large sparse eigenvalue problems.

**Example 1.** Let a circular computational domain be $\Omega = \{(r, \theta) : 0 \leq r \leq R_O, 0 \leq \theta < 2\pi\}$ with an interface $\Gamma = \{(r, \theta) : r = R_I, 0 \leq \theta < 2\pi\}$. The eigenpairs $(\lambda, u)$ of the model problem (1) are given by $u(x, y) = R(r)\Theta(\theta)$,

$$\Theta(\theta) = d_1 \cos m\theta + d_2 \sin m\theta,$$

$$R(r) = \begin{cases} c_1^+ J_m\left(\sqrt{\frac{\lambda}{\beta^+}} r\right) + c_2^+ Y_m\left(\sqrt{\frac{\lambda}{\beta^+}} r\right), & R_I < r \leq R_O, \\ c_1^- J_m\left(\sqrt{\frac{\lambda}{\beta^-}} r\right), & 0 \leq r \leq R_I, \end{cases}$$

where $c_i^{\pm}$ and $d_i$, $i = 1, 2$ are constants, and $J_m$ and $Y_m$ the Bessel functions of the first and second kind of order $m$, respectively. In the Appendix, we explain in more detail how the coefficients $c_i^{\pm}$, $d_i$ could be determined. We set $R_O = 1$, $R_I = 0.38$ and $(\beta^-, \beta^+) = (1, 1000), (1000, 1)$. It seems to be good to choose $\sigma$ dependent on $\beta$, say $\sigma = \kappa\beta$ for some $\kappa \geq 0$. The triangulation of the circular domain consists of quasi-regular triangles with the maximal diameter $h$, which may intersect the interface $\Gamma$ as Fig. 5. Tables 1 and 2 show the first ten eigenvalues $\lambda_i$, $i = 1, 2, \ldots, 10$ in increasing order and their rates of convergence. The first columns are the exact values and the other columns are the eigenvalues computed by IFEM for varying $h$. From the second to sixth column, the meshes are generated so that the degree of freedom quadruples, thus $h$ nearly halves. The numbers in parentheses for each column show the order of convergence. We observe that the order of convergence is quadratic and there are no spurious eigenvalues. Fig. 8 illustrates two eigenfunctions corresponding to eigenvalues $\lambda_1$ and $\lambda_2$ in the case of $\beta^- = 1$, $\beta^+ = 1000$. The cases with other values of $R_I$ and $\beta$ show similar results, although we do not present here.

Now we investigate the influence of penalty parameter $\sigma$ in (9). Numerical results with various choices of $\sigma$ are depicted in Figs. 6 and 7.We observe the optimal convergence of eigenfunctions which are corresponding to $\lambda_1$, $\lambda_2$, $\lambda_4$ together with the case of $\sigma = 0$ in Fig. 7. For all the results in Fig. 7, the second and first order convergence of eigenfunctions in $L^2$ norm and energy norm with respect to $H_h(\Omega)$ are clearly shown. This confirms that the IFEM (including the case of $\sigma = 0$) satisfies the following approximation properties for eigenfunction $u$,

$$\inf_{v_h \in \widehat{N}_h(\Omega)} \|u - v_h\|_{0,\Omega} \leq C_1 h^2 \|u\|_{\widetilde{H}^2(\Omega)}, \qquad \inf_{v_h \in \widehat{N}_h(\Omega)} \|u - v_h\|_{1,J} \leq C_2 h \|u\|_{\widetilde{H}^2(\Omega)},$$

**Table 1**
Eigenvalues computed by IFEM in Fig. 5 when coefficients $\beta^- = 1$, $\beta^+ = 1000$ and penalty parameter $\sigma = \beta$. (ord) in the first row represents the convergence rate.

| $\lambda_{exact}$ | $h = 1/2^5$ (ord) | $h = 1/2^6$ (ord) | $h = 1/2^7$(ord) | $h = 1/2^8$(ord) | $h = 1/2^9$(ord) |
|---|---|---|---|---|---|
| 39.972 | 40.018 (2.11) | 39.982 (2.15) | 39.974 (1.99) | 39.972 (2.08) | 39.972 (1.99) |
| 101.523 | 101.744 (2.40) | 101.566 (2.33) | 101.533 (2.02) | 101.525 (2.12) | 101.523 (2.17) |
| 101.523 | 101.772 (2.52) | 101.573 (2.31) | 101.534 (2.18) | 101.525 (2.13) | 101.523 (2.18) |
| 182.473 | 183.212 (2.64) | 182.626 (2.27) | 182.507 (2.18) | 182.481 (2.20) | 182.475 (2.25) |
| 182.473 | 183.522 (2.56) | 182.636 (2.68) | 182.507 (2.27) | 182.481 (2.16) | 182.475 (2.27) |
| 210.604 | 211.120 (1.82) | 210.723 (2.11) | 210.635 (1.96) | 210.612 (2.00) | 210.606 (2.00) |
| 281.713 | 283.846 (2.54) | 282.098 (2.46) | 281.792 (2.29) | 281.730 (2.18) | 281.716 (2.28) |
| 281.713 | 284.413 (2.67) | 282.140 (2.66) | 281.798 (2.32) | 281.731 (2.25) | 281.717 (2.29) |
| 340.329 | 341.615 (2.00) | 340.625 (2.11) | 340.404 (1.98) | 340.347 (2.06) | 340.333 (2.08) |
| 340.329 | 341.799 (2.16) | 340.643 (2.22) | 340.405 (2.04) | 340.347 (2.05) | 340.333 (2.09) |
| D.O.F | 14 744 | 59 386 | 232 605 | 932 343 | 3 732 735 |

**Table 2**
Eigenvalues computed by IFEM in Fig. 5 when coefficients $\beta^- = 1000$, $\beta^+ = 1$ and penalty parameter $\sigma = \beta$. (ord) in the first row represents the convergence rate.

| $\lambda_{exact}$ | $h = 1/2^5$ (ord) | $h = 1/2^6$ (ord) | $h = 1/2^7$(ord) | $h = 1/2^8$(ord) | $h = 1/2^9$(ord) |
|---|---|---|---|---|---|
| 6.047 | 6.049 (2.01) | 6.047 (1.99) | 6.047 (2.00) | 6.047 (1.98) | 6.047 (1.98) |
| 27.355 | 27.380 (2.35) | 27.360 (2.33) | 27.356 (2.19) | 27.355 (2.13) | 27.355 (2.46) |
| 27.355 | 27.382 (2.42) | 27.360 (2.36) | 27.356 (2.26) | 27.355 (2.12) | 27.355 (2.46) |
| 34.126 | 34.175 (2.49) | 34.135 (2.44) | 34.128 (2.24) | 34.126 (2.13) | 34.126 (2.33) |
| 34.126 | 34.183 (2.42) | 34.136 (2.54) | 34.128 (2.28) | 34.126 (2.16) | 34.126 (2.35) |
| 39.742 | 39.766 (2.08) | 39.748 (1.99) | 39.744 (2.03) | 39.743 (1.96) | 39.742 (2.01) |
| 45.091 | 45.171 (2.12) | 45.104 (2.54) | 45.094 (2.21) | 45.091 (2.11) | 45.091 (2.23) |
| 45.091 | 45.176 (2.62) | 45.106 (2.44) | 45.094 (2.27) | 45.091 (2.17) | 45.091 (2.27) |
| 59.871 | 59.968 (2.40) | 59.890 (2.31) | 59.875 (2.17) | 59.872 (2.09) | 59.871 (2.17) |
| 59.871 | 59.990 (2.21) | 59.892 (2.50) | 59.875 (2.20) | 59.872 (2.14) | 59.871 (2.17) |
| D.O.F | 14 744 | 59 386 | 232 605 | 932 343 | 3 732 735 |

where $C_1$ and $C_2$ are positive constants independent of interface location under the assumptions (H1) and (H2) . The results show non-pollution and completeness of eigenspace, and an optimal convergence order. Fig. 6 illustrates convergence behavior of eigenvalues $\lambda_1, \lambda_2, \lambda_4, \lambda_6$. For some eigenvalues such as $\lambda_2, \lambda_4$ in Fig. 6, we observe that the rates of convergence oscillate. Despite such oscillatory rates, the average convergence order of eigenvalues is roughly quadratic (see Fig. 6). We added the penalty term in (9) to avoid such fluctuations. For small values of $\sigma$, fluctuations in the convergence order of eigenvalues are observed (see $\lambda_2, \lambda_4$ in Fig. 6). If we choose large values of $\sigma$, absolute values of errors become larger since the dependence of $\sigma$ for the constants $C$ in Theorem 5.1 becomes dominant. Based on a variety of numerical experiments, we observe robust convergence behaviors for eigenvalues in the cases of $\sigma = \beta, 10\beta, 100\beta$.

**Example 2.** Let a computational domain be $\Omega = [-1, 1]^2$ and a star-shaped interface is given by $\Gamma = \{(x, y) : \sqrt{x^2 + y^2} - 0.2\sin(5\theta - \pi/5) + 0.5 = 0\}$, where $\theta = \tan^{-1}(y/x)$. In this example, we consider the model problem (1) with variable coefficients. The coefficients $\beta^{\pm}(x, y)$ are given as follows:

$$\beta^-(x, y) = 10 + 5\cos(xy + 10), \qquad \beta^+(x, y) = x^2 + y^2.$$

Our computation is performed on a uniform mesh in Fig. 9. Since the exact eigenvalues are not available, we use the numerical results on a sufficiently refined mesh with mesh size $h = 2^{-10}$ as the reference eigenvalues for the purpose of estimating the orders. Table 3 contains errors of the eigenvalues $\lambda_h$ with various mesh size $h$. We display some eigenfunctions in Fig. 10.

**Example 3.** We consider the problem (1) with a straight-line interface. Let subdomains $\Omega^-$ and $\Omega^+$ be

$$\Omega^- := \{(x, y) : y < 0.5x - 0.2\}, \qquad \Omega^+ := \{(x, y) : y > 0.5x - 0.2\}. \tag{14}$$

The example of mesh for this experiment is shown in Fig. 9. Table 4 shows the first ten eigenvalues and their rates of convergence in the case of $(\beta^-, \beta^+) = (100, 1)$. The reference solutions in the first column are computed from very fine mesh size $h = 2^{-10}$. The results in Table 4 are in good agreement with our theoretical analysis in the previous sections. We display eigenfunctions of $\lambda_1$ and $\lambda_3$ in Fig. 11.

## 7. Conclusion

In this paper, we present an elliptic eigenvalue problem with an interface and adapt a $P_1$-nonconforming IFEM whose analysis for source problems is established in [17]. The spectral analysis starts from formulating the eigenvalue problem

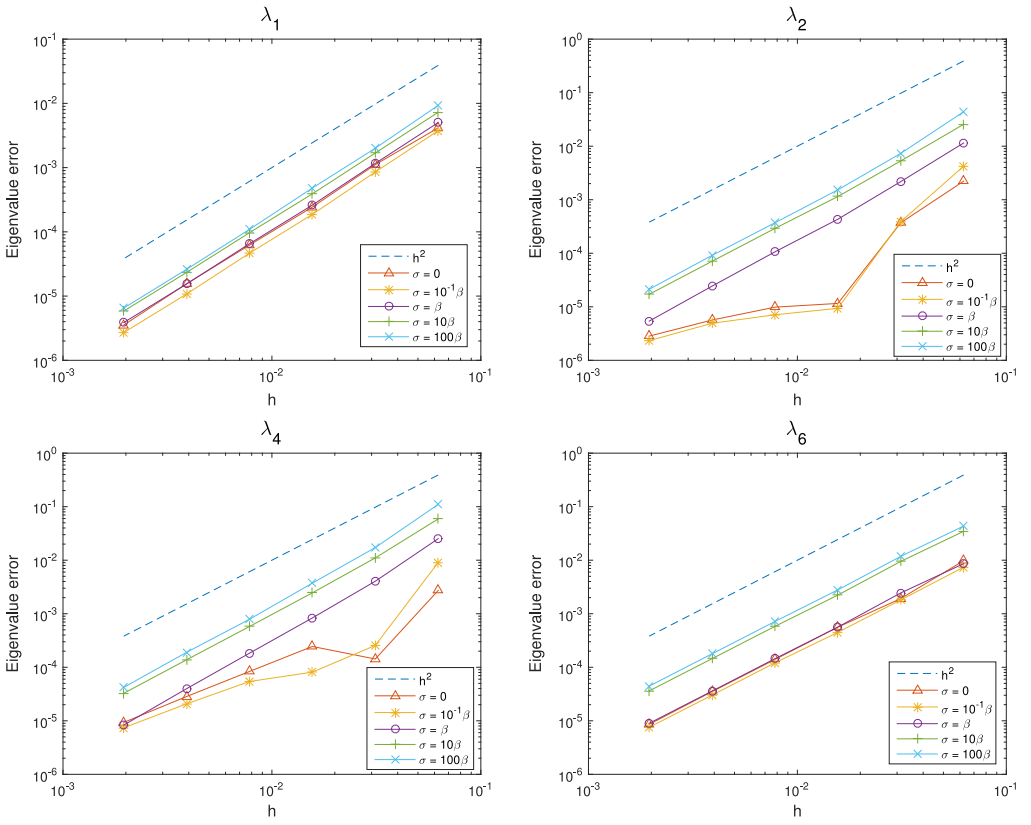


**Fig. 6.** The log–log plot of mesh size $h$ versus the relative error of eigenvalues $\lambda_1$, $\lambda_2$, $\lambda_4$, $\lambda_6$ with penalty parameter $\sigma = 0$ (triangle), $\sigma = 10^{-1}\beta$ (asterisk), $\sigma = \beta$ (circle), $\sigma = 10\beta$ (plus sign) and $\sigma = 100\beta$ (cross). The broken line represents the convergence rate.

**Table 3**
First ten eigenvalues calculated by IFEM in Example 2 in the case of variable coefficients $\beta^-(x, y) = 10 + 5\cos(xy + 10)$, $\beta^+(x, y) = x^2 + y^2$. The reference eigenvalues $\lambda_{ref}$ in the first column are computed with mesh size $h = 1/2^{10}$. The numbers in parentheses show convergence rates. (ord) in the first row represents the convergence rate.

| $\lambda_{ref}$ | $h = 1/2^4$ (ord) | $h = 1/2^5$ (ord) | $h = 1/2^6$ (ord) | $h = 1/2^7$ (ord) | $h = 1/2^8$ (ord) |
|---|---|---|---|---|---|
| 4.139 | 4.183 (2.11) | 4.150 (2.04) | 4.142 (1.99) | 4.140 (2.25) | 4.139 (2.23) |
| 16.502 | 17.052 (1.93) | 16.643 (1.97) | 16.534 (2.10) | 16.509 (2.17) | 16.503 (2.30) |
| 16.605 | 17.153 (1.93) | 16.736 (2.07) | 16.631 (2.30) | 16.611 (2.22) | 16.606 (2.50) |
| 19.868 | 20.515 (2.11) | 20.029 (2.01) | 19.902 (2.21) | 19.876 (2.10) | 19.869 (2.24) |
| 22.901 | 23.722 (1.89) | 23.096 (2.07) | 22.947 (2.09) | 22.911 (2.12) | 22.903 (2.19) |
| 26.898 | 27.636 (1.96) | 27.078 (2.03) | 26.941 (2.05) | 26.907 (2.13) | 26.900 (2.19) |
| 31.158 | 32.454 (1.81) | 31.498 (1.93) | 31.237 (2.11) | 31.175 (2.16) | 31.161 (2.29) |
| 32.267 | 33.546 (1.88) | 32.560 (2.13) | 32.338 (2.04) | 32.282 (2.20) | 32.270 (2.35) |
| 36.817 | 38.398 (1.88) | 37.201 (2.04) | 36.908 (2.07) | 36.837 (2.12) | 36.821 (2.18) |
| 38.376 | 40.009 (1.91) | 38.775 (2.03) | 38.466 (2.14) | 38.396 (2.15) | 38.380 (2.27) |

**Table 4**
First ten eigenvalues calculated by IFEM in Example 3 in the case of coefficients $\beta^- = 100$, $\beta^+ = 1$. The reference eigenvalues $\lambda_{ref}$ in the first column are computed with mesh size $h = 1/2^{10}$. The numbers in parentheses show convergence rates. (ord) in the first row represents the convergence rate.

| $\lambda_{ref}$ | $h = 1/2^4$ (ord) | $h = 1/2^5$ (ord) | $h = 1/2^6$ (ord) | $h = 1/2^7$ (ord) | $h = 1/2^8$ (ord) |
|---|---|---|---|---|---|
| 16.246 | 16.384 (1.98) | 16.277 (2.19) | 16.254 (1.98) | 16.248 (2.11) | 16.247 (2.06) |
| 29.327 | 29.765 (1.99) | 29.417 (2.28) | 29.350 (1.99) | 29.332 (2.11) | 29.328 (2.05) |
| 43.906 | 44.798 (1.99) | 44.092 (2.26) | 43.953 (1.99) | 43.917 (2.10) | 43.908 (2.05) |
| 47.775 | 49.002 (2.00) | 48.050 (2.16) | 47.845 (1.99) | 47.792 (2.07) | 47.779 (2.06) |
| 62.893 | 64.720 (1.98) | 63.258 (2.32) | 62.984 (2.01) | 62.914 (2.11) | 62.898 (2.05) |
| 70.654 | 73.191 (1.98) | 71.207 (2.20) | 70.792 (2.00) | 70.686 (2.07) | 70.661 (2.06) |
| 84.750 | 87.997 (1.99) | 85.412 (2.29) | 84.913 (2.02) | 84.788 (2.10) | 84.759 (2.06) |
| 89.980 | 93.757 (2.00) | 90.848 (2.12) | 90.197 (2.00) | 90.032 (2.06) | 89.992 (2.06) |
| 97.993 | 103.090 (1.99) | 99.116 (2.18) | 98.274 (2.00) | 98.060 (2.07) | 98.009 (2.06) |
| 110.748 | 116.059 (1.99) | 111.834 (2.29) | 111.015 (2.02) | 110.810 (2.10) | 110.763 (2.06) |

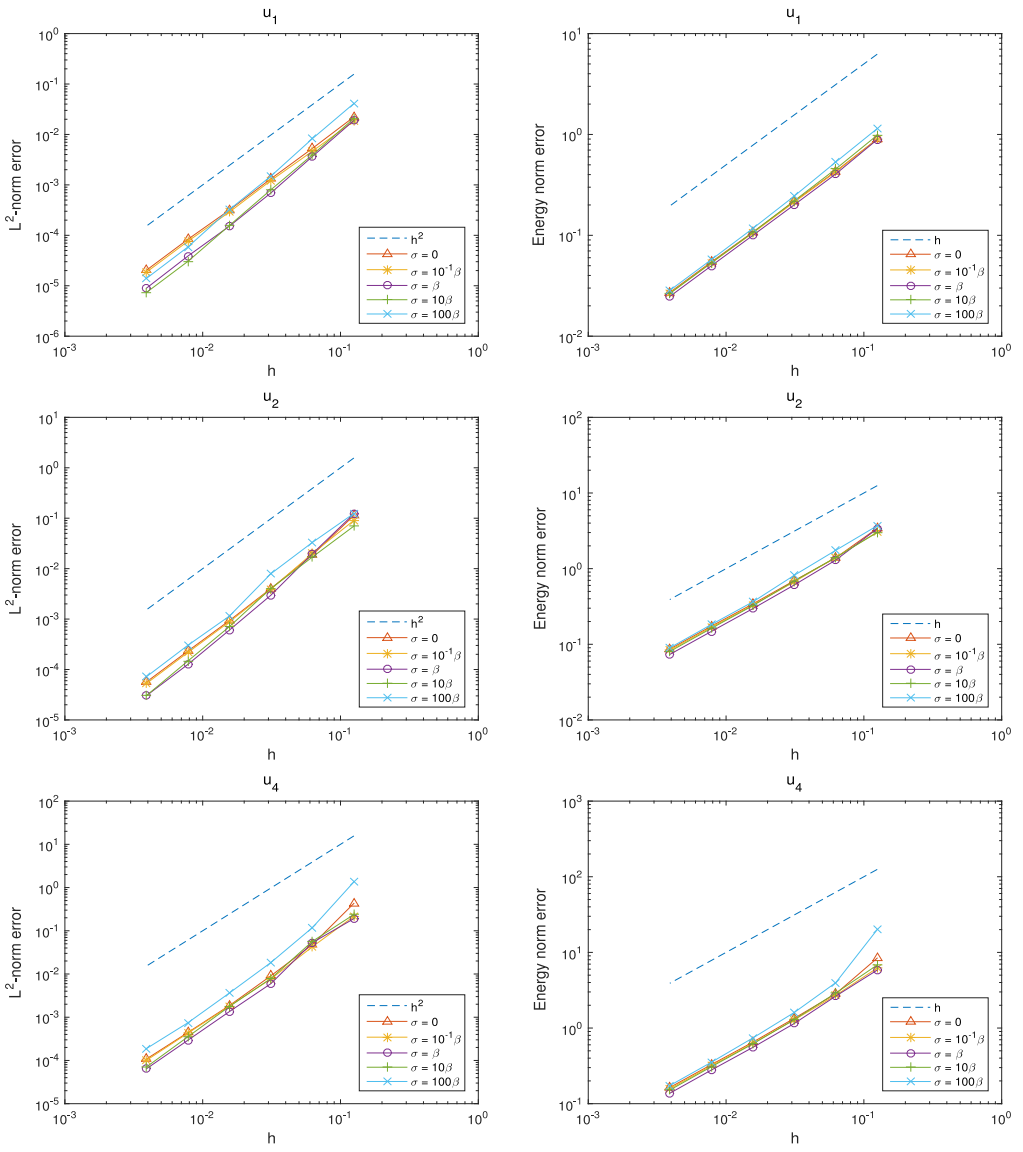


**Fig. 7.** The log–log plot of mesh size $h$ versus the error of eigenfunctions $u_i$ corresponding to $\lambda_i$, $i = 1, 2, 4$ with penalty parameter $\sigma = 0$ (triangle), $\sigma = 10^{-1}\beta$ (asterisk), $\sigma = \beta$ (circle), $\sigma = 10\beta$ (plus sign) and $\sigma = 100\beta$ (cross). The broken line represents the convergence rate. Top row: error of eigenfunction $u_1$; middle row: error of eigenfunction $u_2$; bottom row: error of eigenfunction $u_4$.

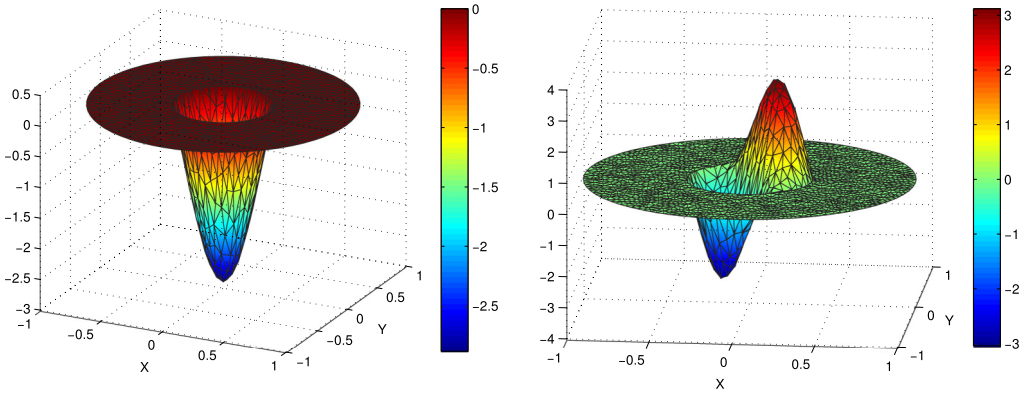


**Fig. 8.** Eigenfunctions corresponding to eigenvalues $\lambda_1$ and $\lambda_2$ in Example 1 in the case of $(\beta^-, \beta^+) = (1, 1000)$.

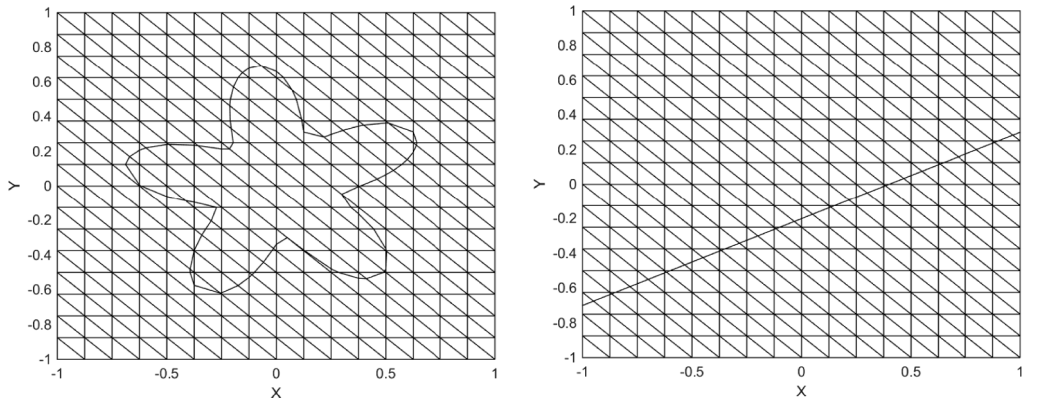


**Fig. 9.** Star-shaped interface and straight-line interface.

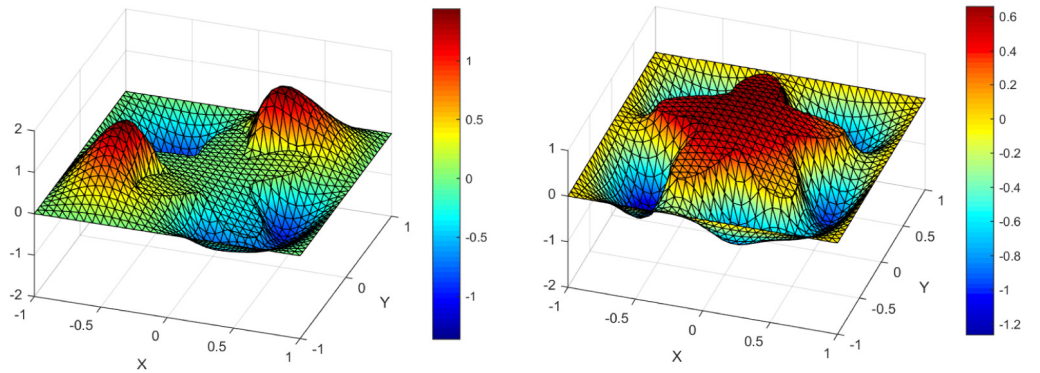


**Fig. 10.** Eigenfunctions corresponding to eigenvalues $\lambda_4$ and $\lambda_6$ in Example 2.

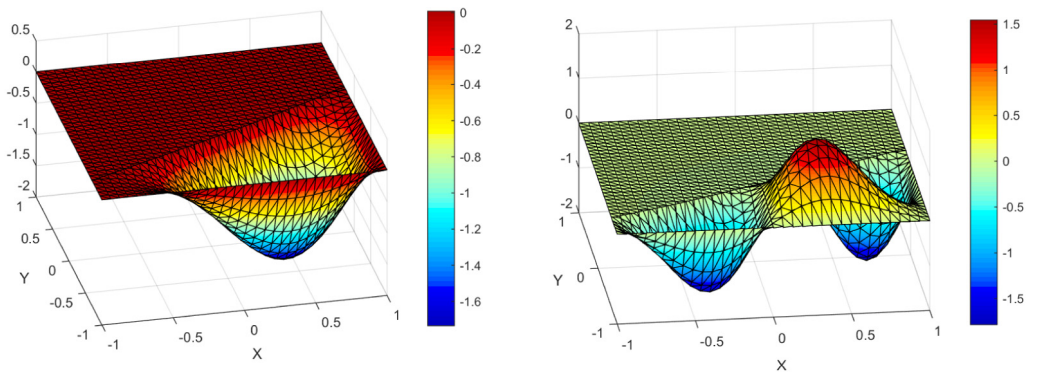


**Fig. 11.** Eigenfunctions corresponding to eigenvalues $\lambda_1$ and $\lambda_3$ in Example 3.

with interface in terms of a solution operator. By using the fact that the solution operator is compact, we show the spectral correctness of IFEM; non-pollution and completeness of the spectrum, and non-pollution and completeness of the eigenspace. Also, an optimal order of convergence for eigenvalues is derived by the approximation properties of IFEM. A series of numerical results with various shapes of interface verify our theoretical results. We observe that the order of convergence for eigenvalues is quadratic. Moreover, we present the optimal convergence of eigenfunctions in the example where the analytic eigensolutions are available. Finally, the method can be applied to the numerical study of stability analysis which plays an important role in many physical problems involving interface. In particular, the results of this paper can be extended to analyze a vibration of composite elastic membranes [48], phase transitions in solid–liquid systems [49], and incompressible flows subject to moving interfaces and rigid boundaries [12,22].

## Acknowledgment

Do Y. Kwak is supported by National Research Foundation of Korea (NRF), No. 2014R1A2A1A11053889.

## Appendix

We show how the eigenvalues from Example 1 in Section 6 can be determined in an analytical way. Recall the domain $\Omega = \{(r,\theta) : 0 \le r \le R_O, 0 \le \theta < 2\pi\}$ and the interface $\Gamma = \{(r,\theta) : r = R_I, 0 \le \theta < 2\pi\}$. The eigenfunction $u(x,y)$ can be determined by the separation of variables, i.e. $u(x,y) = R(r)\Theta(\theta)$. The model problem (1) is rewritten in polar coordinates as follows:

$$\frac{\partial^2 R}{\partial r^2}\Theta + \frac{1}{r}\frac{\partial R}{\partial r}\Theta + \frac{1}{r^2}R\frac{\partial^2 \Theta}{\partial \theta^2} = -\frac{\lambda}{\beta}R\Theta \quad \text{in } \Omega^s,\ s = \pm, \tag{A.1}$$

$$[R(r)]_\Gamma = 0, \qquad \left[\beta r \frac{\partial R(r)}{\partial r}\right]_\Gamma = 0, \tag{A.2}$$

$$R(r) = 0 \quad \text{on } \partial\Omega. \tag{A.3}$$

A reformulation of Eq. (A.1) is

$$\frac{r^2R'' + rR' + \frac{\lambda}{\beta}r^2R}{R} = -\frac{\Theta''}{\Theta} = m^2 \quad \text{in } \Omega^s,\ s = \pm. \tag{A.4}$$

The second relation in (A.4) gives $\Theta(\theta) = d_1 \cos m\theta + d_2 \sin m\theta$. It also establishes that $m$ is an integer since we must have the same value at $\theta = 0$ and $\theta = 2\pi$. The first relation in (A.4) is the Bessel equation

$$r^2R'' + rR' + \left(\frac{\lambda}{\beta}r^2 - m^2\right)R = 0 \text{ in } \Omega^s, \quad s = \pm.$$

Recall that $\beta$ and $\lambda$ are positive by the properties of the model problem (1). We obtain $R(r)$ as follows:

$$R(r) = \begin{cases} c_1^+ J_m\left(\sqrt{\frac{\lambda}{\beta^+}}r\right) + c_2^+ Y_m\left(\sqrt{\frac{\lambda}{\beta^+}}r\right), & \text{in } \Omega^+, \\ c_1^- J_m\left(\sqrt{\frac{\lambda}{\beta^-}}r\right) + c_2^- Y_m\left(\sqrt{\frac{\lambda}{\beta^-}}r\right), & \text{in } \Omega^-, \end{cases}$$

where $J_m$ and $Y_m$ are the Bessel functions of the first and second kind of order $m$. Since $J_m$ is analytic and $Y_m$ is singular at the origin, we have $c_2^- = 0$. The coefficients $c_1^+, c_2^+, c_1^-$ are determined by (A.2) and (A.3). The condition (A.3) leads to the equation

$$c_1^+ J_m\left(\sqrt{\frac{\lambda}{\beta^+}}R_O\right) + c_2^+ Y_m\left(\sqrt{\frac{\lambda}{\beta^+}}R_O\right) = 0. \tag{A.5}$$

By using the first relation of (A.2), we obtain the equation

$$c_1^+ J_m\left(\sqrt{\frac{\lambda}{\beta^+}}R_I\right) + c_2^+ Y_m\left(\sqrt{\frac{\lambda}{\beta^+}}R_I\right) = c_1^- J_m\left(\sqrt{\frac{\lambda}{\beta^-}}R_I\right). \tag{A.6}$$

The second part of (A.2) gives

$$\beta^+\left(c_1^+\frac{d}{dr}\left(J_m\left(\sqrt{\frac{\lambda}{\beta^+}}r\right)\right) + c_2^+\frac{d}{dr}\left(Y_m\left(\sqrt{\frac{\lambda}{\beta^+}}r\right)\right)\right) = \beta^- c_1^-\frac{d}{dr}\left(J_m\left(\sqrt{\frac{\lambda}{\beta^-}}r\right)\right) \quad \text{on } r = R_I. \tag{A.7}$$

From Eqs. (A.5), (A.6), and (A.7), we have a homogeneous matrix equation

$$A\mathbf{c} = 0, \tag{A.8}$$

where

$$A = \begin{bmatrix} J_m\left(\sqrt{\frac{\lambda}{\beta^+}}R_O\right) & Y_m\left(\sqrt{\frac{\lambda}{\beta^+}}R_O\right) & 0 \\ J_m\left(\sqrt{\frac{\lambda}{\beta^+}}R_I\right) & Y_m\left(\sqrt{\frac{\lambda}{\beta^+}}R_I\right) & -J_m\left(\sqrt{\frac{\lambda}{\beta^-}}R_I\right) \\ \beta^+\frac{d}{dr}\left(J_m\left(\sqrt{\frac{\lambda}{\beta^+}}r\right)\right)\Big|_{r=R_I} & \beta^+\frac{d}{dr}\left(Y_m\left(\sqrt{\frac{\lambda}{\beta^+}}r\right)\right)\Big|_{r=R_I} & -\beta^-\frac{d}{dr}\left(J_m\left(\sqrt{\frac{\lambda}{\beta^-}}r\right)\right)\Big|_{r=R_I} \end{bmatrix}$$

and $\mathbf{c} = [c_1^+, c_2^+, c_1^-]^T$. A nonzero solution of (A.8) exists when the determinant of the matrix $A$ is zero. For each index $m$, the eigenvalues $\lambda$ from (A.1) coincide with the roots of the determinant of the matrix $A$, which can be easily calculated by any root-finding method such as bisection method.

## References


[1] B. Deka, T. Ahmed, Convergence of finite element method for linear second-order wave equations with discontinuous coefficients, Numer. Methods Partial Differential Equations 29 (2013) 1522–1542.
[2] C. Zhang, R.J. LeVeque, The immersed interface method for acoustic wave equations with discontinuous coefficients, Wave Motion 25 (1997) 237–263.
[3] S. Badia, R. Codina, A combined nodal continuous-discontinuous finite element formulation for the Maxwell problem, Appl. Math. Comput. 218 (2011) 4276–4294.
[4] R. Hiptmair, J. Li, J. Zou, Convergence analysis of finite element methods for $H(curl; \Omega)$-elliptic interface problems, Numer. Math. 122 (2012) 557–578.
[5] C.S. Peskin, Numerical analysis of blood flow in the heart, J. Comput. Phys. 25 (1977) 220–252.
[6] C.S. Peskin, The immersed boundary method, Acta Numer. 11 (2002) 479–517.
[7] R. Mittal, G. Iaccarino, Immersed boundary methods, Annu. Rev. Fluid Mech. 37 (2005) 239–261.
[8] N. Moës, J. Dolbow, T. Belytschko, A finite element method for crack growth without remeshing, Internat. J. Numer. Methods Engrg. 46 (1999) 131–150.
[9] T.P. Fries, T. Belytschko, The extended/generalized finite element method: An overview of the method and its applications, Internat. J. Numer. Methods Engrg. 84 (2010) 253–304.
[10] R.J. LeVeque, Z. Li, The immersed interface method for elliptic equations with discontinuous coefficients and singular sources, SIAM J. Numer. Anal. 31 (1994) 1019–1044.
[11] Z. Li, T. Lin, X. Wu, New Cartesian grid methods for interface problems using the finite element formulation, Numer. Math. 96 (2003) 61–98.
[12] S. Adjerid, N. Chaabane, T. Lin, An immersed discontinuous finite element method for Stokes interface problems, Comput. Methods Appl. Mech. Engrg. 293 (2015) 170–190.
[13] D.Y. Kwak, S. Jin, D.H. Kyeong, A stabilized $P_1$ immersed finite element method for the interface elasticity problems, arXiv:1408.4227.
[14] T. Lin, D. Sheen, X. Zhang, A locking-free immersed finite element method for planar elasticity interface problems, J. Comput. Phys. 247 (2013) 228–247.
[15] S.H. Chou, D.Y. Kwak, K.T. Wee, Optimal convergence analysis of an immersed interface finite element method, Adv. Comput. Math. 33 (2010) 149–168.
[16] S. Hou, X.D. Liu, A numerical method for solving variable coefficient elliptic equation with interfaces, J. Comput. Phys. 202 (2005) 411–445.
[17] D.Y. Kwak, K.T. Wee, K.S. Chang, An analysis of a broken $P_1$-nonconforming finite element method for interface problems, SIAM J. Numer. Anal. 48 (2010) 2117–2134.
[18] Z. Li, T. Lin, Y. Lin, R.C. Rogers, An immersed finite element space and its approximation capability, Numer. Methods Partial Differential Equations 20 (2004) 338–367.
[19] K.S. Chang, D.Y. Kwak, Discontinuous bubble scheme for elliptic problems with jumps in the solution, Comput. Methods Appl. Mech. Engrg. 200 (2011) 494–508.
[20] Y. Gong, B. Li, Z. Li, Immersed-interface finite-element methods for elliptic interface problems with nonhomogeneous jump conditions, SIAM J. Numer. Anal. 46 (2008) 472–495.
[21] D.N. Arnold, F. Brezzi, Mixed and nonconforming finite element methods: implementation, postprocessing and error estimates, RAIRO Modél. Math. Anal. Numér. 19 (1985) 7–32.
[22] M. Crouzeix, P.A. Raviart, Conforming and nonconforming finite element methods for solving the stationary Stokes equations I, Rev. Fr. Autom. Inform. Rech. Oper. 7 (1973) 33–75.
[23] M.G. Larson, A posteriori and a priori error analysis for finite element approximations of self-adjoint elliptic eigenvalue problems, SIAM J. Numer. Anal. 38 (2000) 608–625.
[24] S. Giani, I.G. Graham, A convergent adaptive method for elliptic eigenvalue problems, SIAM J. Numer. Anal. 47 (2009) 1067–1091.
[25] E.A. Dari, R.G. Durán, C. Padra, A posteriori error estimates for non-conforming approximation of eigenvalue problems, Appl. Numer. Math. 62 (2012) 580–591.
[26] D. Boffi, Approximation of eigenvalues in mixed form, discrete compactness property, and application to hp mixed finite elements, Comput. Methods Appl. Mech. Engrg. 196 (2007) 3672–3681.
[27] D. Boffi, F. Brezzi, L. Gastaldi, On the problem of spurious eigenvalues in the approximation of linear elliptic problems in mixed form, Math. Comp. 69 (2000) 121–140.
[28] B. Mercier, J.E. Osborn, J. Rappaz, P.A. Raviart, Eigenvalue approximation by mixed and hybrid methods, Math. Comp. 36 (1981) 427–453.
[29] I. Babuška, J.E. Osborn, Eigenvalue Problems, in: Handb. Numer. Anal., vol. II, North-Holland, Amsterdam, 1991.
[30] J.E. Osborn, Spectral approximation for compact operators, Math. Comp. 29 (1975) 712–725.
[31] J. Descloux, N. Nassif, J. Rappaz, On spectral approximation. I. The problem of convergence, RAIRO Anal. Numér. 12 (1978) 97–112.
[32] J. Descloux, N. Nassif, J. Rappaz, On spectral approximation. II. Error estimates for the Galerkin method, RAIRO Anal. Numér. 12 (1978) 113–119.
[33] P.F. Antonietti, A. Buffa, I. Perugia, Discontinuous Galerkin approximation of the Laplace eigenproblem, Comput. Methods Appl. Mech. Engrg. 195 (2006) 3483–3503.
[34] R.A. Adams, J.J.F. Fournier, Sobolev Spaces, second ed., Elsevier, Amsterdam, 2003.
[35] J.H. Bramble, J.T. King, A finite element method for interface problems in domains with smooth boundaries and interfaces, Adv. Comput. Math. 6 (1996) 109–138.
[36] O.A. Ladyženskaja, V.J. Rivkind, N.N. Ural'ceva, Solvability of diffraction problems in the classical sense, Tr. Mat. Inst. Steklova 92 (1966) 116–146.
[37] J.W. Barrett, C.M. Elliott, Fitted and unfitted finite-element methods for elliptic equations with smooth interfaces, IMA J. Numer. Anal. 7 (1987) 283–300.
[38] G. Strang, G. Fix, An Analysis of the Finite Element Method, second ed., Wellesley-Cambridge Press, Wellesley, MA, 2008.
[39] J.H. Bramble, J.T. King, A robust finite element method for nonhomogeneous Dirichlet problems in domains with curved boundaries, Math. Comp. 63 (1994) 1–17.

[40] M. Vanmaele, A. Ženíšek, External finite element approximations of eigenvalue problems, RAIRO Modél. Math. Anal. Numér. 27 (1993) 565–589.
[41] E. Hernández, R. Rodríguez, Finite element approximation of spectral problems with Neumann boundary conditions on curved domains, Math. Comp. 72 (2003) 1099–1115.
[42] S. Adjerid, M. Ben-Romdhane, T. Lin, Higher degree immersed finite element methods for second-order elliptic interface problems, Int. J. Numer. Anal. Model. 11 (2014) 541–566.
[43] S. Adjerid, T. Lin, A *p*th degree immersed finite element for boundary value problems with discontinuous coefficients, Appl. Numer. Math. 59 (2009) 1303–1321.
[44] D.N. Arnold, An interior penalty finite element method with discontinuous elements, SIAM J. Numer. Anal. 19 (1982) 742–760.
[45] T. Kato, Perturbation Theory for Linear Operators, in: Classics in Mathematics, Springer-Verlag, Berlin, 1995.
[46] J.B. Conway, A Course in Functional Analysis, second ed., Springer-Verlag, Berlin, 1990.
[47] R.B. Lehoucq, D.C. Sorensen, C. Yang, ARPACK Users' Guide: Solution of Large-Scale Eigenvalue Problems with Implicitly Restarted Arnoldi Methods, SIAM, Philadelphia, 1998.
[48] L.M. Cureton, J.R. Cureton, Eigenvalues of the Laplacian on regular polygons and polygons resulting from their dissection, J. Sound Vib. 220 (1999) 83–98.
[49] J. Prüss, G. Simonett, Stability of equilibria for the Stefan problem with surface tension, SIAM J. Math. Anal. 40 (2008) 675–698.